Sensors and Materials, Vol. 19, No. 6 (2007) 347-363
MYU Tokyo

S & M 0688

Nitrogen Oxide Gas Sensor Based on Multivalent Ion-Conducting Solids

Shinji Tamura and Nobuhito Imanaka*

Department of Applied Chemistry, Faculty of Engineering, Osaka University,
2-1 Yamadaoka, Suita, Osaka 565-0871, Japan

(Received July 27, 2007; accepted August 20, 2007)

Key words: sensor, NO_x, aluminum ion, potassium nitrate, cubic rare-earth oxide

Two types of noble nitrogen oxide gas sensor were fabricated by combining Al^{3+}-ion-conducting $(Al_{0.2}Zr_{0.8})_{20/19}Nb(PO_4)_3$ solid electrolyte and cubic rare-earth oxide-potassium nitrate solid solution as an auxiliary sensing electrode. Since the two sensors applying the oxide-anion-conducting yttria-stabilized zirconia or the aluminum metal as the reference material showed theoretical and quantitative NO gas sensing properties at 450 and 250°C, respectively, it was found that, by changing the reference material, the present sensors using the $(Al_{0.2}Zr_{0.8})_{20/19}Nb(PO_4)_3$ solid electrolyte are promising NO gas sensing devices over a wide temperature range from 250 to 450°C.

1. Introduction

Atmospheric nitrogen oxides (NO_x) mainly comprise nitrogen monoxide (NO) and nitrogen dioxide (NO_2) and are the main cause of acid precipitants. A large amount of NO is emitted from both vehicles and power plants, and the suppression of NO emissions into the atmosphere is an urgent issue. For effective suppression, it is essential to control the NO emissions from individual sites. Although *in situ* devices monitoring the NO gas concentration are required at every emitting site for achieving the above purpose, at present, most of such devices are instruments based on IR absorption and chemical luminescence. These instruments can detect the exact NO_x gas concentration, but some pretreatment of the sample gas is inevitable. Furthermore, these instruments are expensive and they are too large to use at every emitting site. Such disadvantages illustrate the necessity of developing NO_x gas sensing tools that can realize *in situ* monitoring.

Until now, various types of compact solid-state NO_x gas sensors such as those using semiconductors,[1–8] solid electrolytes,[9–13] and organic compounds[14–18] have

*Corresponding author: e-mail: imanaka@chem.eng.osaka-u.ac.jp

been proposed with the purpose of overcoming the above disadvantages. Among them, sensors using organic compounds have potentially low thermal stability, which is inappropriate for high-temperature NO_x gas sensing. Although semiconductor-type sensors show a quick response, they have the disadvantages of low selectivity and low quantitative detection for NO_x gas in the atmosphere, where various types of gas species exist, because the sensing mechanism of the semiconductor-type sensor is based on the electrical resistivity change caused by gas adsorption on the semiconductor surface. On the other hand, solid-electrolyte gas sensors offer the merits of both selective and quantitative gas detection for NO_x gas in addition to rapid and accurate sensing characteristics due to a unique characteristic of the solid electrolyte, that is, only a single ion species can migrate in the solid. This outstanding feature of the solid electrolyte greatly contributes to the selective detection of specific gas species. From our previous studies on the solid-electrolyte gas sensors,[19–34] we have reported the superiority of multivalent-cation-conducting solid electrolytes as the key component of sensors providing excellent sensing performance. Among the multivalent-cation-conducting solids we have developed, the Al^{3+}-ion-conducting $(Al_{0.2}Zr_{0.8})_{20/19}Nb(PO_4)_3$ solid electrolyte[35,36] is considered to be the most suitable candidate for the gas sensor component from the viewpoint of its high ionic conductivity, chemical and thermal stability, and low cost.

In this article, we introduce NO gas sensors with the Al^{3+}-ion-conducting $(Al_{0.2}Zr_{0.8})_{20/19}Nb(PO_4)_3$ solid electrolyte as a key component of the sensor. Furthermore, we have successfully developed chemically and thermally stable K^+-ion-conducting solids based on the cubic rare-earth oxide R_2O_3-KNO_3 (R: rare earth) solid solution, in which KNO_3 exists in the interstitial open spaces in the R_2O_3 lattice. Since this solid contains NO_3^- anions in the cubic structure, it is expected that it can be used as an auxiliary sensing electrode for the NO gas sensor. Here, we fabricated two types of NO gas sensors that can operate at different temperature regions. One is a high-temperature-operation conventional sensor[37,38] whose structure is similar to that of the CO_2 gas sensor we have previously reported,[29,33,34] and another is a low-temperature-operation sensor[39] whose electrical resistance was intentionally reduced by changing the reference material from the highly resistive oxide-ion-conducting yttria-stabilized zirconia to aluminum metal, and their NO gas sensing properties were investigated.

2. Materials and Methods

The $(Al_{0.2}Zr_{0.8})_{20/19}Nb(PO_4)_3$ solid electrolyte was prepared from the starting materials of $Al(OH)_3$, $ZrO(NO_3)_2{\cdot}2H_2O$, Nb_2O_5, and $(NH_4)_2HPO_4$ in a mixing ratio of 8:32:19:114. Powders of these materials were mixed in an agate pot at a rotation speed of 300 rpm for 6 h using planetary ball-milling apparatus (P-7, Fritsch GmbH). The mixed powder was shaped into a pellet and heated at 1000°C for 12 h, 1200°C for 12 h, and then 1300 °C for 12 h in air. After identification of the sample by X-ray powder diffraction (XRD) analysis (Multiflex, Rigaku), the sample was sintered at 1300°C for 12 h in air. Yttria-stabilized zirconia (YSZ: $(ZrO_2)_{0.92}$-$(Y_2O_3)_{0.08}$) was prepared by mixing ZrO_2 and Y_2O_3 in a molar ratio of 92:8, and the mixed powder was pelletized and calcined at 1600°C for 12

h in air. After grinding the sample, the powder was repelletized and sintered at 1600°C for 12 h in air.

Solid $(Nd_{0.6}Gd_{0.4})_2O_3$ was synthesized by coprecipitation using oxalic acid. A stoichiometric solution of 1 mol·L^{-1} $Gd(NO_3)_3$ and 1 mol·L^{-1} $Nd(NO_3)_3$ was added dropwise to 0.5 mol·L^{-1} oxalic acid, and the obtained metal oxalate was heated at 800°C for 12 h. The auxiliary sensing electrode made of R_2O_3-KNO_3 solid solution (R = Gd or $Nd_{0.6}Gd_{0.4}$) was obtained by a conventional solid-state reaction between R_2O_3 and KNO_2 (for R = Gd) or KNO_3 (for R = $Nd_{0.6}Gd_{0.4}$). Powders of these materials were mixed in an appropriate ratio, and then the mixture was ball-milled in an agate pot at a rotation speed of 300 rpm for 6 h. The mixed powder was pelletized and calcined at 450°C for 12 h for the Gd_2O_3-KNO_3 system, and at 400°C for 12 h for the $(Nd_{0.6}Gd_{0.4})_2O_3$-KNO_3 system. After the identification of the obtained sample by XRD analysis and the use of a Fourier transform (FT) IR spectrometer (FT/IR-430, JASCO International Co., Ltd.), the sample pellets were sintered at the same conditions as those of the calcination. The K^+ ion conductivity of the R_2O_3-KNO_3 solids was measured by the complex impedance method using a sintered sample pellet sandwiched by Au bulk electrodes.

We fabricated two types of sensor element. Figure 1 shows schematic illustrations of the NO_x gas sensors with (a) the Gd_2O_3-KNO_3 system and (b) the $(Nd_{0.6}Gd_{0.4})_2O_3$-KNO_3 system as the auxiliary sensing electrode. For the former sensor (Fig. 1(a)), two solid electrolyte pellets of $(Al_{0.2}Zr_{0.8})_{20/19}Nb(PO_4)_3$ and YSZ were tightly fixed using an inorganic adhesive (SUMICERAM 17-D, Asahi Chemical Co., Ltd.) and the auxiliary sensing electrode was set on the $(Al_{0.2}Zr_{0.8})_{20/19}Nb(PO_4)_3$ solid surface. For the latter sensor, only $(Al_{0.2}Zr_{0.8})_{20/19}Nb(PO_4)_3$ was used as the solid electrolyte, and aluminum metal was applied as the reference electrode instead of YSZ. The Al metal was covered with platinum-sputtered film to prevent the oxidation of the Al. After fabricating the sensor element, each sensor was set in an electric furnace and heated to the operation temperature of 450°C for the sensor with the Gd_2O_3-KNO_3 system and 250°C for the

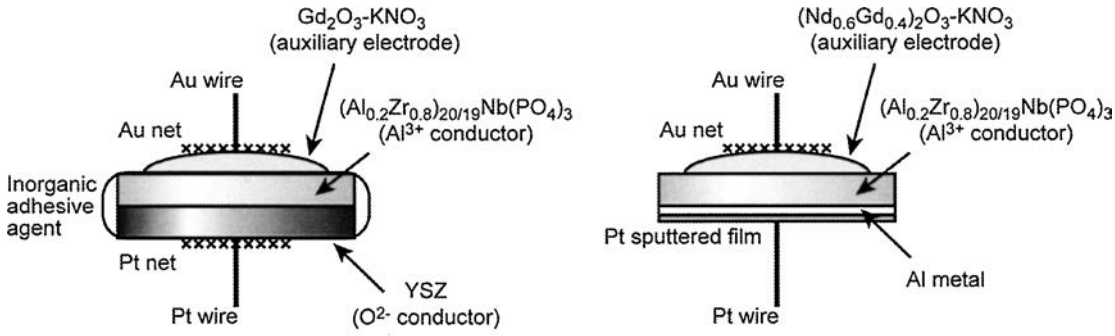

Fig. 1. Schematic illustrations of the NO_x gas sensor with Al^{3+}-ion-conducting $(Al_{0.2}Zr_{0.8})_{20/19}Nb(PO_4)_3$ solid electrolyte and R_2O_3-KNO_3 auxiliary sensing electrode. The reference material applied was (a) O^{2-} ion-conducting yttria-stabilized zirconia (YSZ) and (b) Al metal.

sensor with the $(Nd_{0.6}Gd_{0.4})_2O_3$-KNO_3 system. The NO_x gas concentration was regulated by mixing 1% NO or NO_2 diluted with N_2 gas, and the total gas flow rate was fixed at 100 ml·min^{-1}. The oxygen gas partial pressure (Po_2) was kept constant at 2.1×10^4 Pa. The sensor output (EMF) was monitored using an electrometer (R8240, Advantest).

3. Results and Discussion

3.1. *Sensor based on Al^{3+} and O^{2-} ion conductors with Gd_2O_3-KNO_3 auxiliary sensing electrode*

For the auxiliary sensing electrode of the NO gas sensor, we designed a new material by doping NO_3^- anions into a chemically and thermally stable oxide. Among the various kinds of oxide, rare-earth oxides are promising candidates for realizing the above concept from the viewpoint of their large crystal size. There are three types of crystal structure for rare-earth oxides, namely, A-, B-, and C-type structures. A- and B-type structures have hexagonal and monoclinic symmetries, respectively, and have a comparatively dense structure. On the other hand, the C-type structure is cubic and large interstitial open spaces exist in the structure, which effectively function as spaces where NO_3^- anions can be inserted. Although Eu_2O_3 has the largest lattice volume among the C-type rare-earth oxides, Eu_2O_3 has a demerit regarding practical use, that is, the europium ion sometimes shows a valence change between +3 and +2, resulting in the occurrence of electronic conductivity in the materials. Since this electronic conduction would deteriorate the sensing properties, we selected Gd_2O_3, whose lattice size is second to Eu_2O_3 and shows no valence change, as the auxiliary sensing electrode. In this section, we discuss the performance of the new type of auxiliary sensing electrode, in which NO_3^- anions were doped into Gd_2O_3. Here, we selected KNO_2 as the starting material used to introduce the NO_3^- anions into Gd_2O_3, because KNO_2 shows the highest thermal stability (Table 1) among the alkali-metal nitrites and nitrates, which is an important factor in synthesizing the sample at elevated temperatures. Since KNO_2 is oxidized during the preparation at elevated temperatures, the resulting sample is KNO_3-doped Gd_2O_3.[40, 41]

Figure 2 shows XRD patterns of $(1-x)Gd_2O_3$-$xKNO_3$ ($0.0 \leq x \leq 0.57$) solids. The figure clearly shows that a single phase based on Gd_2O_3 was obtained for samples with

Table 1
Melting points of alkali-metal and nitrates.

Compounds	Temperature/°C
$NaNO_2$	271
KNO_2	440
$LiNO_3$	264
$NaNO_3$	306
KNO_3	339
$RbNO_3$	330
$CsNO_3$	414

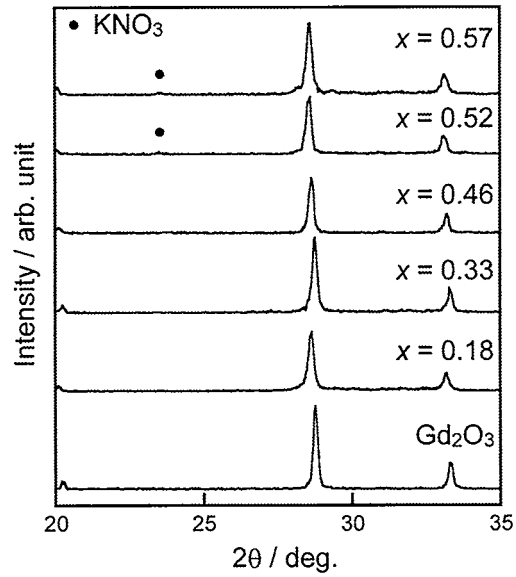

Fig. 2. X-ray powder diffraction patterns of $(1-x)Gd_2O_3$-$xKNO_3$ ($0.0 \leq x \leq 0.57$) solids. (Reprinted with permission from ref. 42. Copyright 2003 Elsevier B.V.)

$x \leq 0.46$. When the KNO_3 content exceeded 0.46, a secondary phase of KNO_3 was observed in addition to the cubic Gd_2O_3 phase. Furthermore, it became clear that the *a* parameter of the cubic Gd_2O_3 phase increased with increasing KNO_3 content up to the solubility limit of $x \leq 0.46$, as listed in Table 2. Since NO_3^- anions were successfully confirmed to exist in the $(1-x)Gd_2O_3$-$xKNO_3$ solids from the FT-IR measurement, it was found that the $(1-x)Gd_2O_3$-$xKNO_3$ ($0.0 \leq x \leq 0.46$) solids could form solid solutions.

To investigate the thermal stability of the $(1-x)Gd_2O_3$-$xKNO_3$ ($0.0 \leq x \leq 0.46$) solid solutions, we carried out thermal gravimetric analysis of the $0.54Gd_2O_3$-$0.46KNO_3$ solid solution (Fig. 3). Although pure KNO_2 (a starting material of the $0.54Gd_2O_3$-$0.46KNO_3$ solid solution) reacts with oxygen in the atmosphere to form KNO_3 at 400 – 600°C and then decomposes to K_2O at around 650°C, the $0.54Gd_2O_3$-$0.46KNO_3$ solid solution shows superior thermal stability up to 700°C without significant weight change. This result also supports the idea that the $0.54Gd_2O_3$-$0.46KNO_3$ solid can successfully form a solid solution.

Figure 4 shows the compositional dependence of the K^+ ion conductivity (The pure K^+ ion conducting behavior has been already demonstrated.[41]) for $(1-x)Gd_2O_3$-$xKNO_3$ ($0.0 \leq x \leq 0.57$) solids at 600°C. By forming $(1-x)Gd_2O_3$-$xKNO_3$ solid solutions for samples with $x \leq 0.46$, the conductivity was shown to monotonically increase with increasing KNO_3 content, and the highest K^+ ion conductivity of 1.72×10^{-1} S·cm^{-1} was obtained at $x = 0.46$. In contrast, the conductivities of the samples with a two-phase mixture ($x > 0.46$) decrease with *x* due to the secondary KNO_3 phase formation.

Table 2
Lattice parameter, a, of the cubic KNO_3-doped Gd_2O_3 solids.

x in $(1-x)Gd_2O_3$-$xKNO_3$	a/nm
0.0	1.08137
0.18	1.08154
0.33	1.08162
0.46	1.08195
0.52	1.08196
0.57	1.08196

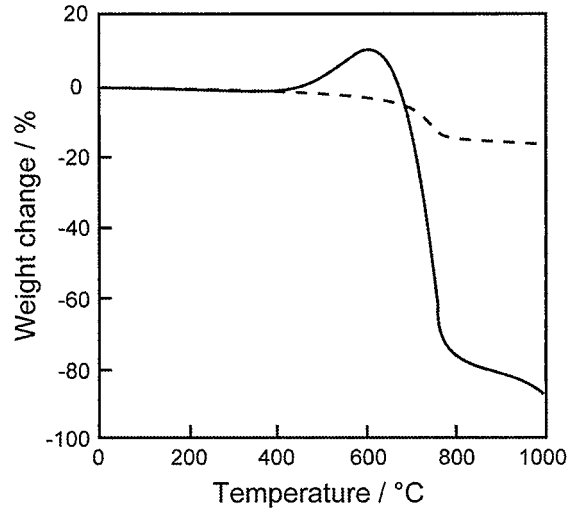

Fig. 3. Thermal gravimetric results of $0.54Gd_2O_3$-$0.46KNO_3$ solid solution (---) and pure KNO_2 (—). (Reprinted with permission from ref. 42. Copyright 2003 Elsevier B.V.)

From these results, we selected the $0.54Gd_2O_3$-$0.46KNO_3$ solid solution, which shows high K^+ ion conductivity as well as high thermal stability, as the auxiliary sensing electrode, and fabricated the NO_x gas sensor element with the structure shown in Fig. 1(a).

Figure 5 shows the typical sensor response curve observed when the NO gas concentration was increased from 200 to 2000 ppm and then reduced to 200 ppm at 450°C, which is a typical NO concentration range in exhaust gases. The response time to the NO gas concentration change, which is defined as the time necessary to attain 90% of the total response, was within 7 min. Furthermore, it was clear that the sensor exhibited a continuous and reproducible response to NO.

The possible reactions that may occur at the auxiliary sensing electrode, the interface between the auxiliary sensing electrode and the Al^{3+} ion conductor, the interface between the two solid electrolytes, and at the reference electrode are as follows.

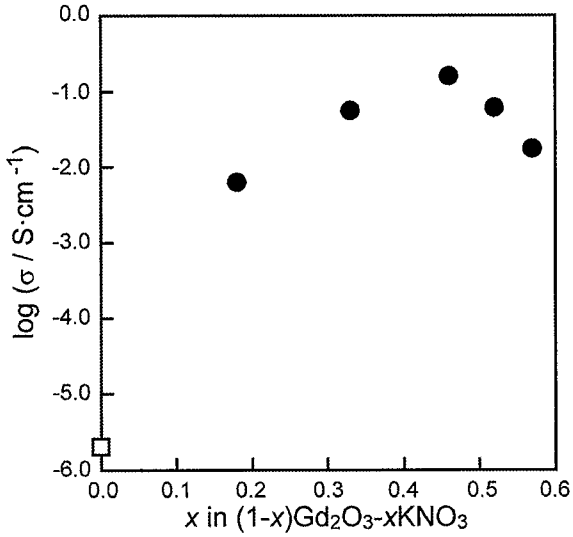

Fig. 4. Compositional dependence of K^+ ion conductivity for $(1-x)Gd_2O_3$-$xKNO_3$ ($0.18 \leq x \leq 0.57$) solids at 600°C. The open square shows the electrical conductivity at 600°C for pure Gd_2O_3. (Reprinted with permission from ref. 42. Copyright 2003 Elsevier B.V.)

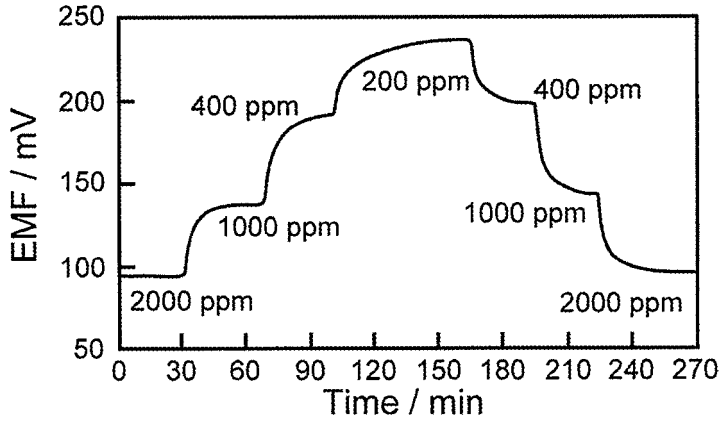

Fig. 5. Typical sensor EMF output variation with increase in NO content from 200 to 2000 ppm then decrease to 200 ppm for the sensor with the $0.54Gd_2O_3$-$0.46KNO_3$ auxiliary sensing electrode at 450°C. (Reprinted with permission from ref. 38. Copyright 2003 Elsevier B.V.)

Auxiliary sensing electrode ($0.54Gd_2O_3$-$0.46KNO_3$):

$$KNO_3 \text{ (in } Gd_2O_3) \leftrightarrow K^+ + NO + O_2^{\uparrow} + e^- \quad (1)$$

Interface between $0.54Gd_2O_3$-$0.46KNO_3$ and $(Al_{0.2}Zr_{0.8})_{20/19}Nb(PO_4)_3$:

$$K^{+} + (19/12)(Al_{0.2}Zr_{0.8})_{20/19}Nb(PO_4)_3 \leftrightarrow (1/3)Al^{3+} + (19/12)(K_{0.6}Zr_{0.8})_{20/19}Nb(PO_4)_3 \quad (2)$$

Interface between $(Al_{0.2}Zr_{0.8})_{20/19}Nb(PO_4)_3$ and YSZ:

$$(1/3)Al^{3+} + (1/2)O^{2-} \leftrightarrow (1/6)Al_2O_3 \quad (3)$$

Reference electrode (YSZ):

$$(1/4)O_2^{II} + e^{-} \leftrightarrow (1/2)O^{2-} \quad (4)$$

Here, O_2^{I} and O_2^{II} represent the oxygen gas on the surfaces of the auxiliary sensing electrode and reference electrode, respectively. From the above reactions, the following full chemical reaction can be written.

$$KNO_3 + (19/12)(Al_{0.2}Zr_{0.8})_{20/19}Nb(PO_4)_3 + (1/4)O_2^{II} \leftrightarrow NO + O_2^{I} + (19/12)(K_{0.6}Zr_{0.8})_{20/19}Nb(PO_4)_3 + (1/6)Al_2O_3 \quad (5)$$

Then, the Nernst equation can be expressed as follows.

$$E = E_0 - (RT/nF)\ln\{(P_{NO})\cdot(Po_2^{I})\cdot(a(K_{0.6}Zr_{0.8})_{20/19}Nb(PO_4)_3)^{19/12}\cdot(aAl_2O_3)^{1/6}\cdot(aKNO_3)^{-1}\cdot(a(Al_{0.2}Zr_{0.8})_{20/19}Nb(PO_4)_3)^{-19/12}\cdot(Po_2^{II})^{-1/4}\} \quad (6)$$

In eq. (6), E_0 is constant and the number of electrons (n) is 1.00. The *a* and P terms represent the activity of the solid materials and the partial pressure of the gas species, respectively. Since the activity of the solid is constant at a certain temperature and the oxygen gas pressure in the test gas is kept constant at 2.1×10^4 Pa, eq. (6) can be simplified to

$$E = E_0' - (RT/nF)\ln(P_{NO}) \qquad (E_0'\text{: constant, n = 1.00}). \quad (7)$$

Figure 6 presents the sensor EMF output observed in Fig. 5 as a function of the logarithm of the NO gas concentration. With increasing NO gas concentration, the sensor EMF output monotonically decreased during the stages of increasing and decreasing NO gas concentration, and a 1:1 linear relationship was clearly observed between the EMF and the logarithm of the NO gas concentration. The theoretical slope calculated from eq. (7) is also depicted in the same figure as a solid line. The values of n estimated from the slope of the measured EMF during increasing and decreasing NO gas concentration are 1.03 and 1.01, respectively, which are extremely close to the theoretical value of 1.00. From this result, it was shown that the sensor combined with the Al^{3+}-ion-conducting $(Al_{0.2}Zr_{0.8})_{20/19}Nb(PO_4)_3$ and YSZ with $0.54Gd_2O_3$-$0.46KNO_3$ as an auxiliary sensing electrode showed the theoretical Nernst response to NO gas concentration.

We also investigated the NO_2 gas sensing characteristics of the sensor with the $0.54Gd_2O_3$-$0.46KNO_3$ auxiliary sensing electrode. For NO_2 gas sensing, the plausible

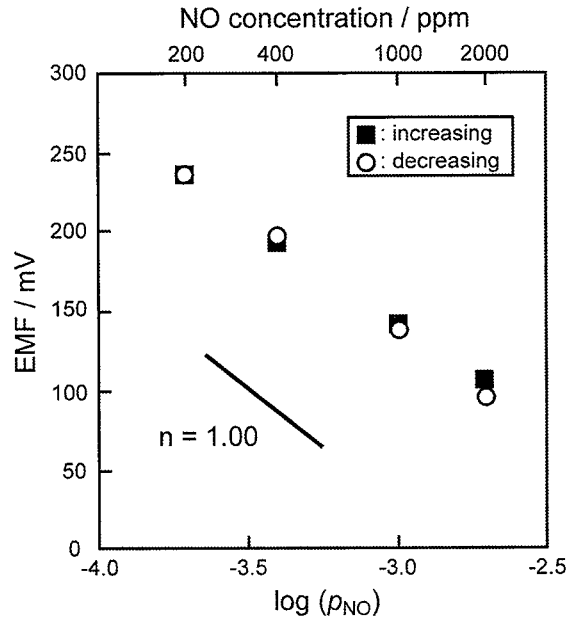

Fig. 6. Relationship between the sensor EMF output and the logarithm of the NO gas concentration for the sensor with the $0.54Gd_2O_3$-$0.46KNO_3$ auxiliary sensing electrode at 450°C. (■: increasing NO gas concentration, ○: decreasing NO gas concentration) (Reprinted with permission from ref. 38. Copyright 2003 Elsevier B.V.)

reaction at the auxiliary sensing electrode given in eq. (1) can be rewritten as the following equation:

$$KNO_3 \text{ (in } Gd_2O_3) \leftrightarrow K^+ + NO_2 + (1/2)O_2^I + e^- \tag{8}$$

and the Nernst equation is similarly given as follows.

$$E = E_0' - (RT/nF)\ln(P_{NO2}) \qquad (E_0'\text{: constant, n = 1.00}) \tag{9}$$

A similar response curve for NO_2 to that for NO (Fig. 5) was obtained and the 90% response time was 10 min, which was slightly slower than that for NO gas sensing. The sensor EMF output variation is displayed in Fig. 7. Similar behavior to that shown in Fig. 6 was observed and the values of n estimated from the slope during increasing and decreasing NO_2 concentration were n = 1.01 and 1.00, respectively. Furthermore, since the EMFs for NO and NO_2 are almost the same, the present sensor is strongly expected to function as an *in situ* total NO_x ($NO + NO_2$) gas sensing device. Figure 8 shows the sensor output deviation when the NO to NO_2 gas content ratio was varied while fixing the total NO_x gas concentration at 2000 ppm. Upon changing the NO:NO_2 ratio from 9:1 to 1:9, no significant EMF deviation was observed, indicating that the present sensor

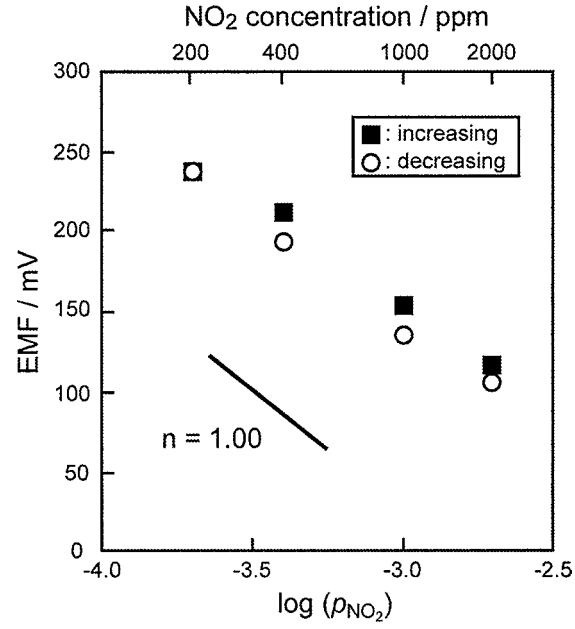

Fig. 7. Relationship between the sensor EMF output and the logarithm of the NO_2 gas concentration for the sensor with the $0.54Gd_2O_3$-$0.46KNO_3$ auxiliary sensing electrode at 450°C. (■: increasing NO_2 gas concentration, ○: decreasing NO_2 gas concentration) (Reprinted with permission from ref. 39. Copyright 2004 The Electrochemical Society, Inc.)

with the $0.54Gd_2O_3$-$0.46KNO_3$ auxiliary sensing electrode can detect the total NO_x gas content independent of the proportions of NO and NO_2.

3.2. *Sensor based on Al^{3+} ion conductor with $(Nd_{0.6}Gd_{0.4})_2O_3$-KNO_3 auxiliary sensing electrode*

There is a demand for practical portable sensors that operate at lower temperatures. However, the sensor with the $(Al_{0.2}Zr_{0.8})_{20/19}Nb(PO_4)_3$ solid electrolyte, YSZ and auxiliary sensing electrode described above could not operate effectively at lower temperatures because of the high electrical resistance of the sensor element below 400°C. Therefore, we designed a new sensor cell by modifying not only the auxiliary sensing electrode but also the material of the sensor element (Fig. 1(b)). Among the proposed materials for the sensor element, YSZ shows the lowest ion conductivity below 400°C (Fig. 9), which is the main reason that the sensor operation is inhibited below 400°C. Therefore, we removed the YSZ from the sensor element. However, since a reference material is necessary to obtain a stable sensor output, we used Al metal as the reference material for the low-temperature-operation sensor.

In our previous study on cubic rare-earth oxides, it was found that the $(Nd_{0.6}Gd_{0.4})_2O_3$ solid has the largest cubic lattice,[42] indicating the largest interstitial open spaces in

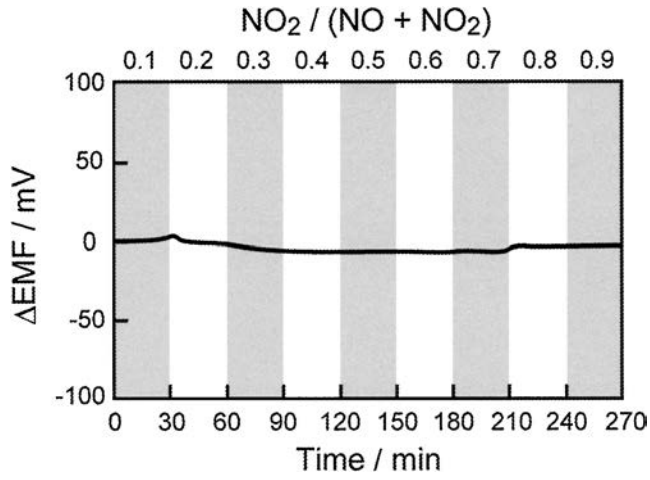

Fig. 8. Sensor EMF output deviation upon changing the NO to NO_2 gas content ratio at 450°C. The total NO_x gas concentration (NO + NO_2) is kept constant at 2000 ppm. (Reprinted with permission from ref. 39. Copyright 2004 The Electrochemical Society, Inc.)

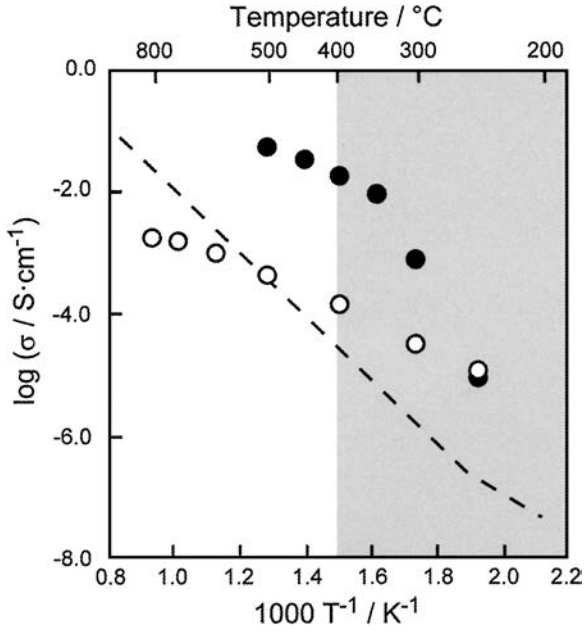

Fig. 9. Temperature dependences of the ion conductivity for the materials used for the sensor element shown in Fig. 1(a); $(Al_{0.2}Zr_{0.8})_{20/19}Nb(PO_4)_3$ solid electrolyte (○), $0.54Gd_2O_3$-$0.46KNO_3$ auxiliary sensing electrode (●) and YSZ (---). The shaded area indicates the temperature region below 400°C.

the cubic rare-earth oxide structure. Therefore, we selected the $(Nd_{0.6}Gd_{0.4})_2O_3$ solid as the cubic rare-earth oxide for the auxiliary sensing electrode of the R_2O_3-KNO_3 system to realize high K^+ ion conductivity at low temperatures. Figure 10 shows the K^+ ion conductivities of the $0.54Gd_2O_3$-$0.46KNO_3$ and $0.55(Nd_{0.6}Gd_{0.4})_2O_3$-$0.45KNO_3$ solids, which contain almost the same amount of KNO_3. As we expected, a higher K^+ ion conductivity was obtained for the $(Nd_{0.6}Gd_{0.4})_2O_3$-based solid, indicating the possibility of a low-temperature-operation sensor using the $(Nd_{0.6}Gd_{0.4})_2O_3$-based solid as the auxiliary sensing electrode.

From the XRD analyses of the $(1-x)(Nd_{0.6}Gd_{0.4})_2O_3$-$x$KNO3 solids ($0.0 \leq x \leq 0.55$), it was clear that a single-phase cubic rare-earth oxide was obtained for the sample with $x \leq 0.45$, and higher KNO_3 content resulted in a two-phase mixture of cubic phase and KNO_3. Figure 11 displays the compositional dependences of the lattice volume and conductivity at 250°C for the $(1-x)(Nd_{0.6}Gd_{0.4})_2O_3$-$xKNO_3$ solids. Similar behavior was observed for the lattice volume and conductivity when the KNO_3 content increased, that is, both the lattice volume and the conductivity of the solid monotonically increased up to $x = 0.45$, and no further changes in both the lattice volume and the conductivity were observed for $x > 0.45$. This result clearly indicates that a solid solution of the cubic rare-earth oxide $(Nd_{0.6}Gd_{0.4})_2O_3$ and KNO_3 was successfully formed in the compositional range of $x \leq 0.45$, and it was found that $0.55(Nd_{0.6}Gd_{0.4})_2O_3$-$0.45KNO_3$ showed a maximum K^+ ion conductivity of 3.47×10^{-4} S·cm^{-1} at 250°C.

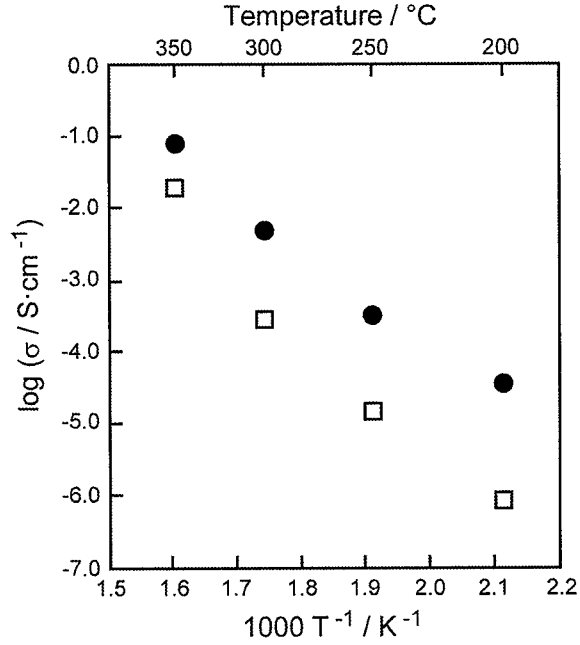

Fig. 10. Temperature dependences of the K^+ ion conductivity for the $0.55(Nd_{0.6}Gd_{0.4})_2O_3$-$0.45KNO_3$ solid solution (●) and the $0.54Gd_2O_3$-$0.46KNO_3$ solid solution (□).

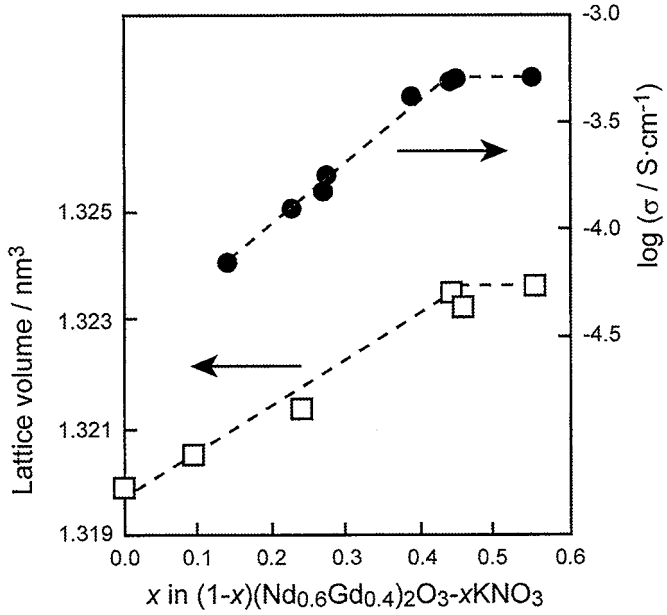

Fig. 11. Compositional dependences of lattice volume and conductivity at 250°C for the $(1-x)(Nd_{0.6}Gd_{0.4})_2O_3$-$xKNO_3$ solids.

Figure 12 depicts a representative sensor response curve obtained by varying the NO gas concentration from *ca.* 200 to 2000 ppm and then reducing it to 200 ppm at 250°C. Since the 90% response time was less than 5 min, it was demonstrated that the present sensor showed a rapid, continuous and reproducible response to NO gas even at temperatures as low as 250°C.

The plausible reactions at the auxiliary sensing electrode, the interface between the auxiliary sensing electrode and the Al^{3+}-ion-conducting $(Al_{0.2}Zr_{0.8})_{20/19}Nb(PO_4)_3$ solid, and the reference electrode of Al metal are as follows.

Auxiliary sensing electrode:

$$KNO_3 \text{ (in } (Nd_{0.6}Gd_{0.4})_2O_3) \leftrightarrow K^+ + NO + O_2 + e^- \quad (10)$$

Interface between the auxiliary sensing electrode and the $(Al_{0.2}Zr_{0.8})_{20/19}Nb(PO_4)_3$ solid:

$$K^+ + (19/12)(Al_{0.2}Zr_{0.8})_{20/19}Nb(PO_4)_3 \leftrightarrow (1/3)Al^{3+} + (19/12)(K_{0.6}Zr_{0.8})_{20/19}Nb(PO_4)_3 \quad (11)$$

Reference electrode of Al metal:

$$(1/3)Al^{3+} + e^- \leftrightarrow Al \quad (12)$$

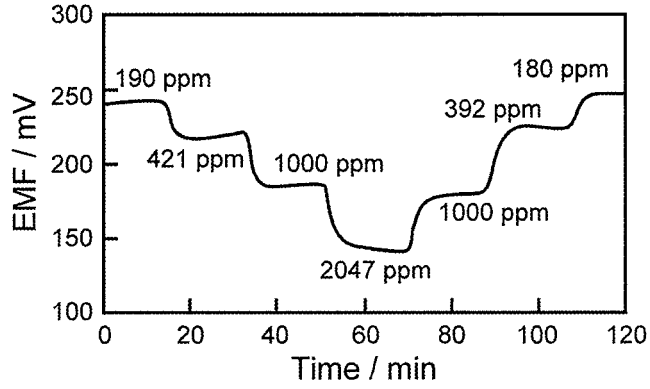

Fig. 12. Representative sensor response curve observed upon increasing the NO gas concentration from 200 to 2000 ppm and then decreasing it to 200 ppm at 250°C for the sensor with Al metal reference electrode and $0.55(Nd_{0.6}Gd_{0.4})_2O_3$-$0.45KNO_3$ auxiliary sensing electrode. (Reprinted with permission from ref. 40. Copyright 2006 American Scientific Publishers)

From eqs. (10) to (12), the full chemical reaction can be expressed as follows.

$$KNO_3 + (19/12)(Al_{0.2}Zr_{0.8})_{20/19}Nb(PO_4)_3 \leftrightarrow Al + (19/12)(K_{0.6}Zr_{0.8})_{20/19}Nb(PO_4)_3 + NO + O_2 \quad (13)$$

The chemical reaction in eq. (13) leads to the following Nernst equation.

$$E = E_0 - (RT/nF)\ln\{(a\mathrm{Al})(a(K_{0.6}Zr_{0.8})_{20/19}Nb(PO_4)_3)^{19/12}(P_{NO})(Po_2)(a\mathrm{KNO_3})^{-1}(a(Al_{0.2}Zr_{0.8})_{20/19}Nb(PO_4)_3)^{-19/12}\} \quad (14)$$

Here, n = 1.00, and Po_2 is constant at 2.1×10^4 Pa, the same as for the high-temperature-operation sensor. Therefore, eq. (14) is simplified to

$$E = E_0\text{''} - (RT/nF)\ln(P_{NO}) \qquad (E_0\text{''}: \text{constant, n} = 1.00). \quad (15)$$

The sensor EMF output in Fig. 12 for increasing and decreasing NO gas concentration is plotted in Fig. 13 as closed squares and open circles, respectively. The EMF increased with decreasing NO gas concentration, and a linear relationship was observed between the sensor EMF output and the logarithm of the NO gas concentration. The values of n estimated from the slope for increasing and decreasing NO concentration are 1.07 and 1.03, respectively, and these values are extremely close to the calculated theoretical value (n = 1.00), indicating that the present sensor shows the theoretical Nernst response to NO gas even at 250°C.

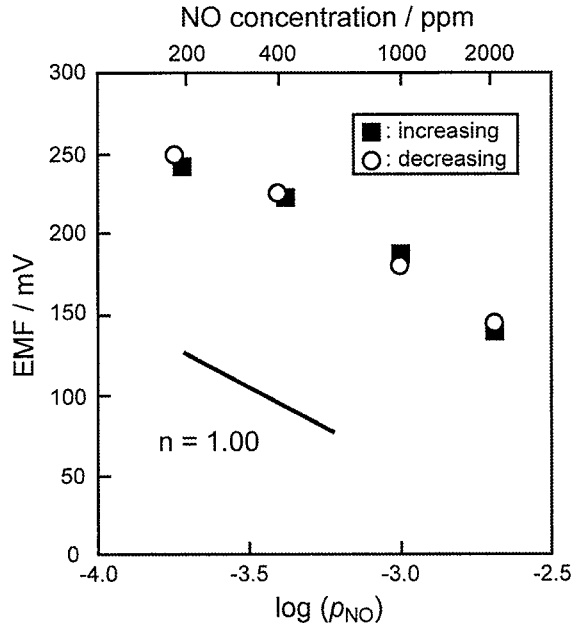

Fig.13. Sensor EMF variation for increasing (■) and decreasing (○) NO gas concentration at 250°C for the sensor with Al metal reference electrode and $0.55(Nd_{0.6}Gd_{0.4})_2O_3$-$0.45KNO_3$ auxiliary sensing electrode. (Reprinted with permission from ref. 40. Copyright 2006 American Scientific Publishers)

4. Conclusions

Two types of smart NO_x gas sensor were successfully developed by the combination of the trivalent Al^{3+}-ion-conducting solid electrolyte $(Al_{0.2}Zr_{0.8})_{20/19}Nb(PO_4)_3$ and the cubic rare-earth-oxide-based auxiliary sensing electrode, R_2O_3-KNO_3 (R = Gd, $Nd_{0.6}Gd_{0.4}$) solid solution. The sensor with Al^{3+}-cation- and oxide-anion-conducting solids and $0.54Gd_2O_3$-$0.46KNO_3$ solid solution as an auxiliary sensing electrode exhibited a superior gas sensing performance, such as rapid, continuous and reproducible responses to NO gas at 450°C. Furthermore, this sensor could also measure not only individual NO and NO_2 concentrations but also the total NO_x ($NO+NO_2$) concentration at 450°C. On the other hand, the sensor composed of Al^{3+}-cation-conducting solid and Al metal with $0.55(Nd_{0.6}Gd_{0.4})_2O_3$-$0.45KNO_3$ solid solution as an auxiliary sensing electrode showed excellent sensing performance even at a temperature as low as 250°C by reducing the electrical resistance of the sensor cell. Since such a superior sensing performance was realized over a wide temperature range (250 to 450°C), the present sensors based on the Al^{3+}-ion-conducting solid and R_2O_3-KNO_3 solid solution are strongly expected to be used as practical NO gas monitoring tools that can be utilized at various types of NO gas emitting site.

References

1 Y. Sadaoka, T. A. Jones and W. Göpel: Sens. Actuators B **1** (1990) 148.
2 G. Sberveglieri, S. Groppeli, P. Nelli, V. Lantto, H. Torvela, P. Romppainen and S. Leppavuori: Sens. Actuators B **1** (1990) 79.
3 N. Rao, C. M. van den Bleek and J. Schoonman: Solid State Ionics **59** (1993) 263.
4 M. Akiyama, Z. Zhang, J. Tamaki, N. Miura, N. Yamazoe and T. Harada: Sens. Actuators B **13** (1993) 619.
5 N. Imanaka, S. Banno and G. Adachi: Chem. Lett. **2** (1994) 319.
6 N. Imanaka, Y. Hirota and G. Adachi: Electrochem. Solid-State Lett. **2** (1999) 100.
7 S. Tanaka and T. Esaka: J. Mater. Res. **16** (2001) 1389.
8 C. Li, D. Zhang, X. Liu, S. Han, T. Tang, J. Han and C. Zhou: Appl. Phys. Lett. **82** (2003) 1613.
9 S. Zhuiykov, T. Ono, N. Yamazoe and N. Miura: Solid State Ionics **152** (2002) 801.
10 M. L. Grilli, E. di Bartolomeo and E. Traversa: J. Electrochem. Soc. **148** (2001) H98.
11 N. Rao, C. M. van den Bleek and J. Schoonman: Solid State Ionics **52** (1992) 339.
12. N. Miura, M. Nakatou and S. Zhuiykov: Electrochem. Commun. **4** (2002) 284.
13 N. Imanaka, T. Yamamoto and G. Adachi: Electrochem. Solid-State Lett. **2** (1999) 409.
14 J. J. Miasik, A. Hooper and B. C. Tofield: J. Chem. Soc. Faraday Trans. **1** (1986) 1117.
15 T. A. Temofonte and K. F. Schoch: J. Appl. Phys. **65** (1989) 1350.
16 Y. Sadaoka, T. A. Jones, G. S. Revell and W. Gopel: J. Mater. Sci. **25** (1990) 5257.
17 C. Hamann, A. Mrwa, M. Muller, W. Gopel and M. Rager: Sens. Actuators B **4** (1991) 73.
18 A. Heilmann, M. Muller, C. Hamann, V. Lantto and H. Torvela: Sens. Actuators B **4** (1991) 511.
19 S. Tamura, N. Imanaka, M. Kamikawa and G. Adachi: Adv. Mater. **12** (2000) 898.
20 N. Imanaka, T. Yamamoto and G. Adachi: Chem. Lett. **29** (2000) 834.
21 N. Imanaka, M. Kamikawa, S. Tamura and G. Adachi: Solid Sate Ionics **133** (2000) 279.
22 N. Imanaka, K. Okamoto and G. Adachi: Electrochem. Commun. **3** (2001) 49.
23 S. Tamura, N. Imanaka, M. Kamikawa and G. Adachi: Sens. Actuators B **73** (2001) 205.
24 N. Imanaka, A. Ogura, M. Kamikawa and G. Adachi: Electrochem. Commun. **3** (2001) 451.
25 N. Imanaka, M. Kamikawa and G. Adachi: Anal. Chem. **74** (2002) 4800.
26 N. Imanaka, K. Okamoto and G. Adachi: Mater. Lett. **57** (2003) 1966.
27 N. Imanaka, A. Ogura and G. Adachi: Electrochemistry **71** (2003) 14.
28 N. Imanaka: Ionics **9** (2003) 36.
29 N. Imanaka, A. Oda, S. Tamura, G. Adachi, T. Maekawa, T. Tsumeishi and H. Ishikawa: Electrochem. Solid-State Lett. **7** (2004) H12.
30 S. Tamura, I. Hasegawa, N. Imanaka, T. Maekawa, T. Tsumeishi, K. Suzuki, H. Ishikawa, A. Ikeshima, Y. Kawabata, N. Sakita and G. Adachi: Sens. Actuators B **108** (2005) 359.
31 N. Imanaka and S. Tamura: Enc. Sensor **2** (2005) 13.
32 T. Maekawa, Y. Kawabata, Y. Nakazato, H. Ishikawa, S. Tamura, N. Imanaka and G. Adachi: Electrochemistry **74** (2006) 118.
33 N. Imanaka, M. Kamikawa, S. Tamura and G. Adachi: Electrochem. Solid-State Lett. **2** (1999) 602.
34 N. Imanaka, M. Kamikawa, S. Tamura and G. Adachi: Sens. Actuators B **77** (2001) 301.
35 N. Imanaka, Y. Hasegawa, M. Yamaguchi, M. Itaya, S. Tamura and G. Adachi: Chem. Mater. **14** (2002) 4481.
36 Y. Hasegawa, S. Tamura and N. Imanaka: J. New Mater. Electrochem. Sys. **8** (2005) 203.
37 A. Oda, N. Imanaka and G. Adachi: Sens. Actuators B **93** (2003) 229.
38 N. Imanaka, A. Oda, S. Tamura and G. Adachi: J. Electrochem. Soc. **151** (2004) H113.

39 N. Imanaka, I. Hasegawa and S. Tamura: Sensor Lett. **4** (2006) 340.
40 Y. W. Kim, T. Masui, A. Oda, S. Tamura and N. Imanaka: Phys. Status Solidi **198** (2003) 369.
41 Y. W. Kim, A. Oda and N. Imanaka: Electrochem. Commun. **5** (2003) 94.
42 S. Tamura, A. Mori and N. Imanaka: Electrochem. Commun. **9** (2007) 245.